Iodide ion as an electron shuttle to significantly accelerate the elimination of sulfamethazine in the Fenton-like system under neutral condition

Junyang Xiao [a,b], Yangju Li [a,b], Haoran Dong [a,b,*], Zijun Pang [c], Mengxi Zhao [a,b], Jie Dong [a,b], Daofen Huang [a,b], Long Li [a,b]

[a] College of Environmental Science and Engineering, Hunan University, Changsha, Hunan 410082, China
[b] Key Laboratory of Environmental Biology and Pollution Control (Hunan University), Ministry of Education, Changsha, Hunan 410082, China
[c] School of Environment and Energy, South China University of Technology, Guangzhou, Guangdong 510006, PR China

ARTICLE INFO

ABSTRACT

In this study, iodide ion (I^-) was introduced as an electron shuttle to significantly accelerate the elimination of sulfamethazine (SMT) with hydrogen peroxide (H_2O_2) activated by amorphous zero-valent iron microsphere (A-mZVI) under neutral condition. Compared with the A-mZVI/H_2O_2 system, the removal efficiency of SMT was improved by 80.8% after supplying with trace amounts of I^-. It was that $^1O_2$ was the primary reactive species responsible for SMT degradation, although $^\bullet OH$, $O_2^{\bullet-}$, $Fe^{IV}O^{2+}$, and hypoiodous acid (HOI) also existed in the A-mZVI/H_2O_2/I^- system. Furthermore, the possible degradation pathways of SMT were recommended, and the toxicity assessment of the degradation intermediates were also conducted. In addition, the influences of some key factors, the application in different water matrix, the degradation performance of some diverse pollutants, and the reusability of A-mZVI were also explored. This study proposed a promising process for improving the Fenton-like reaction under neutral condition by using I^-.

1. Introduction

In the past decades, advanced oxidation processes (AOPs), which could produce reactive oxygen species (ROS) (e.g., singlet oxygen ($^1O_2$), hydroxyl radical ($^\bullet OH$), superoxide radical ($O_2^{\bullet-}$), sulfate radical ($SO_4^{\bullet-}$), and organic radicals (R-O$^\bullet$) with strong oxidation capacity, have achieved remarkable achievements in the elimination of refractory organic contaminants, and are increasingly favored by relevant researchers [1–5]. The Fenton method was extremely representative in AOPs due to the simply operation and environmentally benign characteristics (Eq. (1)) [6]. However, the rate of reduction of Fe^{3+} to Fe^{2+} was rather slow, which becomes the rate-limiting step of the Fenton process [7]. This meant that a large amount of ferrous iron salt was required to maintain the reaction, which will cause loads of iron-containing sludge to be produced and increase the burden of subsequent treatment [8]. To overcome this limitation, researchers have carried out various modifications and improvements to the traditional Fenton reaction, including extending to Fenton-like reaction and heterogeneous Fenton reaction [9–11].

$$Fe^{2+} + H_2O_2 \rightarrow Fe^{3+} + OH^- + {}^\bullet OH \tag{1}$$
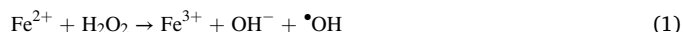
Zero-valent iron (ZVI) has aroused extensive concern owing to its superiorities of easy synthesis, environmentally benign, cost-effective, and can be utilized as an iron source to continuously generate Fe^{2+} species responsible for Fenton reaction from the iron core through corrosion reaction (Eqs. (2–3)) [12]. For example, Bremner et al. reported that the application of ZVI/H_2O_2 process permitted high removal efficiency of phenol (PhOH) by the generation of $^\bullet OH$ [13]. Nevertheless, the surface of ZVI would appear surface passivation under the near-neutral and/or alkaline conditions in the actual water environment, and the precipitated iron (oxy)hydroxide would cover its surface and reduce its catalytic activity [14]. For this shortcoming, researchers have proposed a series of methods to modify ZVI, such as loading on solid supports, sulfidation, surface coating, and doping of the second metal [15–18]. Recently, our research team used amorphous zero-valent iron microspheres (A-mZVI) to activate peroxydisulfate (PDS) and found that the A-mZVI/PDS system exhibited a much better performance on the sulfamethazine (SMT) removal than that of conventional crystalline nanoscale zero-valent iron (C-nZVI) activated PDS system. The reason for this enhanced performance was that the amorphous structure accelerated electron release from the iron core to the surface of A-mZVI

---

* Corresponding author at: College of Environmental Science and Engineering, Hunan University, Changsha, Hunan 410082, China.
E-mail address: dongh@hnu.edu.cn (H. Dong).

to form Fe^{2+} [19].
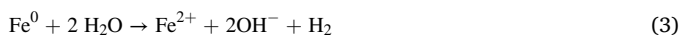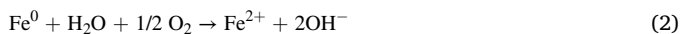
$$Fe^0 + H_2O + 1/2\ O_2 \rightarrow Fe^{2+} + 2OH^- \qquad (2)$$

$$Fe^0 + 2\ H_2O \rightarrow Fe^{2+} + 2OH^- + H_2 \qquad (3)$$

Iodine was a ubiquitously naturally-occurring halogen with an average concentration of about 0.5 mg kg^{-1} in the Earth's crust, 10.0–20.0 ng m^{-3} in the atmosphere, and 0.5–100.0 µg L^{-1} in natural water [20,21]. The ubiquitous iodide (I$^-$) has caused a train of studies on its redox conversion with peroxides such as permanganate, ferrate, peroxomonosulfate (PMS), PDS, and hydrogen peroxide (H$_2$O$_2$) [22–26]. Moreover, during the latest years, the role of iodine in the elimination of organic micro-pollutants also has attracted more and more attention [20,27,28]. During the oxidative water treatment process, I$^-$ could be oxidized to generate reactive iodine species (RIS) by the peroxides, like iodide radical (I$^\bullet$), iodide radical anions (I$_2^{\bullet-}$), triiodide ions (I$_3^-$), iodate (IO$_3^-$), and hypoiodous acid (HOI) [21,27,29]. For example, Feng et al. reported the rapid selective degradation of phenolic pollutants at circumneutral condition by I$^\bullet$ generated in the PMS/I$^-$ system [27]. Given the ubiquitous existence of I$^-$ in natural water, it is wondering whether the combination of I$^-$ and Fenton system (A-mZVI/H$_2$O$_2$/I$^-$) would have the potential to rapidly degrade organic pollutants under neutral conditions? However, to the best of our knowledge, there has been no relevant study on the combination of I$^-$ and Fenton-like system to remove organic pollutants.

SMT was selected as the target pollutant in this study because it was a typical sulfonamide antibiotic, which was frequently detected in water [11]. It was reported that SMT had a potential toxicity risk to ecosystem [30]. In detail, the objectives of this work are to: (i) verify the ability of the established A-mZVI/H$_2$O$_2$/I$^-$ process in SMT removal as a novel AOP under neutral condition; (ii) identify the dominant major reactive species that contributed to SMT elimination and investigate the mechanism of ROS generation; (iii) predict the degradation pathway of SMT by DFT calculation and LC-MS detection and forecast the variation of acute and chronic toxicity of SMT and its intermediates; (iv) study the influence of reaction conditions (e.g., A-mZVI dosage, I$^-$/H$_2$O$_2$ concentration, and initial pH of the reaction system) and coexisting substances (e.g., Cl$^-$, HCO$_3^-$, SO$_4^{2-}$, and humic acid) on SMT removal efficiency; (v) inspect the applicability of A-mZVI/H$_2$O$_2$/I$^-$ system in groundwater and tap water, the reusability of A-mZVI, and the efficiency of degrading other pollutants.

2. Materials and methods

2.1. Chemical reagents

The sources of chemical reagents were shown in Supporting Information (SI, **Text S1**).

2.2. Catalyst synthesis

The synthesis procedure of A-mZVI via liquid phase reduction of FeCl$_2$·4 H$_2$O by NaBH$_4$ in the presence of ethylenediamine (EDA) was similar to that described in our previous work [19].

2.3. Batch experiments

For the catalytic activity test, all the experiments were performed in a constant temperature shaker (TP80C, Jinlan, Shanghai) under the rate of 250 rpm at room temperature (25.0 ± 0.5 °C) for a reaction of 15 min 100 mL predetermined concentration of target pollutant aqueous solution primarily placed in a 250 mL glass bottle. Subsequently, a desired amount of H$_2$O$_2$ stock solution was appended into the above solution, and then the initial pH of solution was regulated rapidly to a specific value via adding 10.0 mM of H$_2$SO$_4$ and/or NaOH. Lastly, the reaction was initiated by introducing the predetermined dosage of A-mZVI and

the desired amount of I$^-$ into the above solution, respectively. Afterwards, 1 mL reaction solution samples were extracted at predetermined intervals, filtered through 0.22 µm membranes immediately and quenched with excess Na$_2$S$_2$O$_3$ for analysis of SMT or other pollutants within 24 h.

2.4. Analytical methods

The detailed information on the analytical methods could be found in SI (**Text S2**).

2.5. Characterizations

The X-ray diffraction (XRD), scanning electron microscope (SEM), X-ray photoelectron spectroscopy (XPS), Tafel polarization curves, and electrochemical impedance spectroscopic (EIS) were used to characterize the synthesized A-mZVI. The detailed characterization information were exhibited in SI (**Text S3**).

2.6. Density functional theory (DFT) calculation method

The details of DFT calculation were presented in SI (**Text S4**).

2.7. Quantitative structure-activity relationship (QASR) assessment

The mutagenicity of SMT and its degradation intermediates were evaluated by using the Toxicity Estimation Software Tool (T.E.S.T.) (version 5.1.2) [31]. The ECOSAR program (version 2.2) was applied to assess the acute and chronic toxicity of SMT and its degradation intermediates toward daphnids, fish, and green algae [32].

3. Results and discussion

3.1. Material characterization

The phase analysis of the synthesized A-mZVI was implemented by employing an X-ray diffractometer (XRD), and obtained phase characteristic patterns were depicted in Fig. S1. There was no obvious diffraction peak at 44.6°, which was consistent with previous research reports, indicating that amorphous structured ZVI was successfully synthesized [33,34]. Furthermore, the element valent sate analysis of synthesized A-mZVI was conducted with an X-ray photoelectron spectrometry (XPS) (Fig. S2). The XPS spectra of Fe 2p displayed a peak belonging to Fe^0 species at 706.9 eV [35], which illustrated the successful synthesis of ZVI. In addition, the XPS spectra of survey scan of synthesized A-mZVI revealed that a small amount of N was detected owing to the introduction of ethylenediamine (EDA) during the synthesis processes [36]. Fig. S3 showed that the synthesized A-mZVI exhibited a spherical structure with a size between 100 to 400 nm. Besides, the synthesized A-mZVI was further analyzed by electrochemical analysis. As shown in Fig. S4, the Tafel polarization curve of A-mZVI with a higher corrosion current of 1.9×10^{-5} A than that of C-nZVI (1.1×10^{-6} A), indicating that the composite of A-mZVI had a superior electron transfer rate and excellent catalytic performance [37]. Moreover, the electrochemical impedance spectroscopy (EIS) test revealed that A-mZVI had a smaller semicircular diameter than that of C-nZVI, which indicated that A-mZVI had a higher charge transfer efficiency and conductive properties (Fig. S5) [38].

3.2. Comparison of different processes on SMT removal

The elimination of SMT in aqueous solutions under different systems, including H$_2$O$_2$, I$^-$, A-mZVI, I$^-$/H$_2$O$_2$, A-mZVI/H$_2$O$_2$, A-mZVI/I$^-$, and A-mZVI/H$_2$O$_2$/I$^-$ at the initial pH of 7.0 are presented in Fig. 1. The removal efficiency of SMT was all less than 5.5% for the individual system (H$_2$O$_2$ system, I$^-$ system, and A-mZVI system) after reaction of
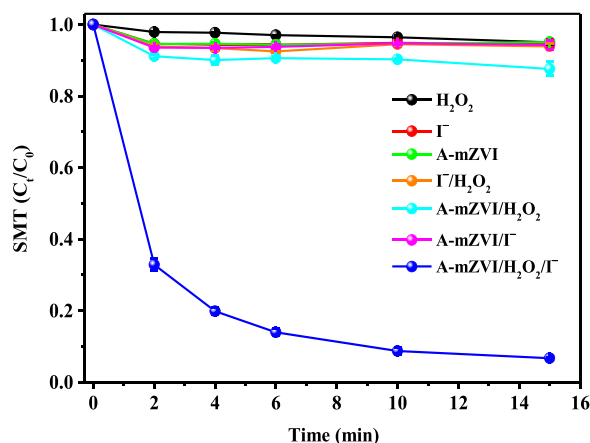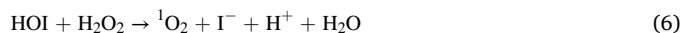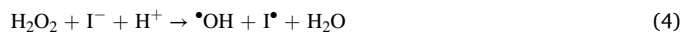
Fig. 1. The removal of SMT in different reaction systems. Reaction conditions: $[SMT]_0 = 10.0$ μM, $[A\text{-}mZVI]_0 = 10.0$ mg L^{-1}, $[I^-]_0 = 15.0$ μM, $[H_2O_2]_0 = 15.0$ μM, $pH_0 = 7.0 \pm 0.1$, and $T = 25.0 \pm 0.5$ °C.

15 min. These results indicated that the adsorption of SMT by A-mZVI alone was very small, H_2O_2 alone showed negligible oxidation of SMT, and I^- also could not degrade SMT directly. Similarly, the removal of SMT by I^-/H_2O_2 and A-mZVI/I^- systems was also inconsiderable. As for the A-mZVI/H_2O_2 system, the removal efficiency of SMT could reach 12.5%, which could be attributed to the fact that A-mZVI could activate H_2O_2 to produce limited amount of ROS to remove SMT under neutral condition. Surprisingly, the removal efficiency of SMT was significantly improved when I^- was added to the A-mZVI/H_2O_2 system (A-mZVI/H_2O_2/I^- system), reaching to 93.3% within 15 min under given conditions. Compared to the pseudo-first-order rate constants (k_{obs}) (Eq. S1) of SMT removal in the A-mZVI/H_2O_2/I^- system and A-mZVI/H_2O_2 system, the k_{obs} of SMT removal in A-mZVI/H_2O_2/I^- (0.1622 min^{-1}) system was about 26.6-fold higher than that in the A-mZVI/H_2O_2 (0.0061 min^{-1}) system (Fig. S6). Therefore, it was most likely that the rapid elimination of SMT in A-mZVI/H_2O_2/I^- system was enhanced due to the synergistic effect of H_2O_2 and I^-.

Meanwhile, the variation of H_2O_2 concentration in A-mZVI/H_2O_2/I^- system during the reaction was determined, and the result was exhibited in Fig. S7. It was found that the concentration of H_2O_2 decreased from 15.0 μM to 5.0 μM with the reaction, which indicated that H_2O_2 was activated by A-mZVI associated with I^- or consumed effectively via other substances in the reaction system. During the elimination of SMT in the A-mZVI/H_2O_2/I^- process, H_2O_2 might be consumed mainly through the following three aspects: one is that the H_2O_2 was consumed during the activation of H_2O_2 by A-mZVI (Eqs. (1–3)), one is consumed by catalytic oxidation of I^- (Eqs. (4–5)), and the other is consumed by rapid reduction of HOI (Eq. 6) [39,40]. Moreover, the amount of Fe leached in the reaction was also measured (Fig. S8), and the concentration of leached Fe only being 0.07 mg L^{-1}, which was met the relevant requirements of the Environmental Quality Standards for Surface Water (GB 3838–2002, China) and Standards for Drinking Water Quality (GB 5749–2022, China). In addition, to interpret the effect of leached iron ions on the system, the elimination of SMT in the $Fe^{2+}/H2O2/I^-$ system (the Fe^{2+} concentration was equal to the leached total iron concentration) was investigated, and the result was summarized in Fig. S9. It was evident that the contribution of the homogeneous system to SMT removal was minor in comparison to that of the A-mZVI/H_2O_2/I^- system, indicating that the primary reaction took place on the surface of A-mZVI. Moreover, the mineralization rate of A-mZVI/H_2O_2/I^- system and A-mZVI/H_2O_2 system were conducted (Fig. S10). The results showed that the mineralization rate of A-mZVI/H_2O_2/I^- system was achieved 39.4%, which was much higher than the 6.5% of the A-mZVI/H_2O_2 system. This phenomenon indicated that the A-mZVI/H_2O_2/I^- process had a good decontamination ability to
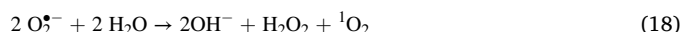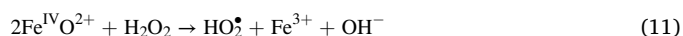
effectively eliminate SMT.

$$H_2O_2 + I^- + H^+ \rightarrow {}^\bullet OH + I^\bullet + H_2O \tag{4}$$

$$I^\bullet + H_2O_2 \rightarrow HOI + {}^\bullet OH + H_2O \tag{5}$$

$$HOI + H_2O_2 \rightarrow {}^1O_2 + I^- + H^+ + H_2O \tag{6}$$

3.3. Removal mechanism of SMT in the AmZVI/I^-/H_2O_2 system

3.3.1. Identification of reactive species

In the H_2O_2 activation system, the ROS might include ${}^\bullet OH$, $O_2^{\bullet-}$, and ${}^1O_2$ according to previous researches [41,42]. Therefore, quenching experiments were conducted by introducing different scavengers into the reaction media to identify the ROS produced in the A-mZVI/H_2O_2/I^- system and the dominant ROS that responsible for SMT elimination. TBA was usually utilized as a quenching agent for ${}^\bullet OH$ owing to the high reaction rate constants for TBA reaction with ${}^\bullet OH$ ($k = (3.8–7.6) \times 10^8$ $M^{-1} s^{-1}$) [17]. As denoted in Fig. 2(a), the elimination of SMT was only slightly dropped when TBA was present in the A-mZVI/H_2O_2/I^- system, indicating that ${}^\bullet OH$ was present in the reaction system (Eqs. (1, 4–5, and 7)), but not the main free radical. For further confirming the role of ${}^\bullet OH$ in the A-mZVI/H_2O_2/I^- system, benzoic acid (BA, $k = 5.9 \times 10^9$ M^{-1} s^{-1}) was used as the typical ${}^\bullet OH$ probe to identify the existence of ${}^\bullet OH$ [43], and the result was shown in Fig. S11. It could also be inferred that ${}^\bullet OH$ acted a minor role in the removal of SMT as no significant elimination of BA was observed with or without TBA. In the meantime, superoxide dismutase (SOD), a typical scavenger for $O_2^{\bullet-}$ ($k = (1.5–3.0) \times 10^8$ $M^{-1} s^{-1}$), was applied to explore whether the $O_2^{\bullet-}$ was generated in the A-mZVI/H_2O_2/I^- system (Eqs. (8–12)) [44]. It was observed that the k_{obs} of SMT removal declined from 0.1622 to 0.0607 min^{-1} in the presence of the SOD (Fig. S12), suggesting that $O_2^{\bullet-}$ was produced in the process. In term of furfuryl alcohol (FFA, a scavenger of ${}^1O_2$, $k = 1.2 \times 10^8$ $M^{-1} s^{-1}$) [45], the degradation of SMT was significantly inhibited by 83.2% within 15 min, which illustrated that ${}^1O_2$ may devote a great contribution to the removal of SMT in the A-mZVI/H_2O_2/I^- system (Eqs. (6, 13–18)) [40,43,46].

$$Fe^{IV}O^{2+} + H_2O \rightarrow {}^\bullet OH + Fe^{3+} + OH^- \tag{7}$$

$$H_2O_2 + {}^\bullet OH \rightarrow H_2O + HO_2^\bullet \tag{8}$$

$$I_2^{\bullet-} + H_2O_2 \rightarrow 2I^- + HO_2^\bullet + H^+ \tag{9}$$

$$Fe^{3+} + H_2O_2 \rightarrow HO_2^\bullet + Fe^{2+} + H \tag{10}$$

$$2Fe^{IV}O^{2+} + H_2O_2 \rightarrow HO_2^\bullet + Fe^{3+} + OH^- \tag{11}$$

$$HO_2^\bullet \leftrightarrow O_2^{\bullet-} \text{ (pH dependent)} \tag{12}$$

$$O_2^{\bullet-} + {}^\bullet OH \rightarrow OH^- + {}^1O_2 \tag{13}$$

$$O_2^{\bullet-} + HO_2^\bullet \rightarrow HO_2^- + {}^1O_2 \tag{14}$$

$$HO_2^- + {}^{H2O2} \rightarrow H_2O + OH^- + {}^1O_2 \tag{15}$$

$${}^{HO2\bullet} \rightarrow H^+ + {}^1O_2 \tag{16}$$

$$HO_2^\bullet + HO2^\bullet \rightarrow H_2O + {}^1O_2 \tag{17}$$

$$2 O_2^{\bullet-} + 2 H_2O \rightarrow 2OH^- + H_2O_2 + {}^1O_2 \tag{18}$$

According to the previous studies, $Fe^{IV}O^{2+}$ may present in addition to ${}^\bullet OH$ in the Fenton process at neutral and/or alkaline pH values (Eq. (19)) [46]. $Fe^{IV}O^{2+}$ could react with PMSO to form PMSO$_2$ via two-electron transfer reaction [47]. Therefore, PMSO was utilized to confirm whether $Fe^{IV}O^{2+}$ was generated in the A-mZVI/H_2O_2/I^- system, the result was shown in Fig. S13. A small amount of PMSO was transformed into PMSO$_2$ during the reaction, indicating that there was a trace amount of $Fe^{IV}O^{2+}$ was formed in the A-mZVI/H_2O_2/I^- process, and its
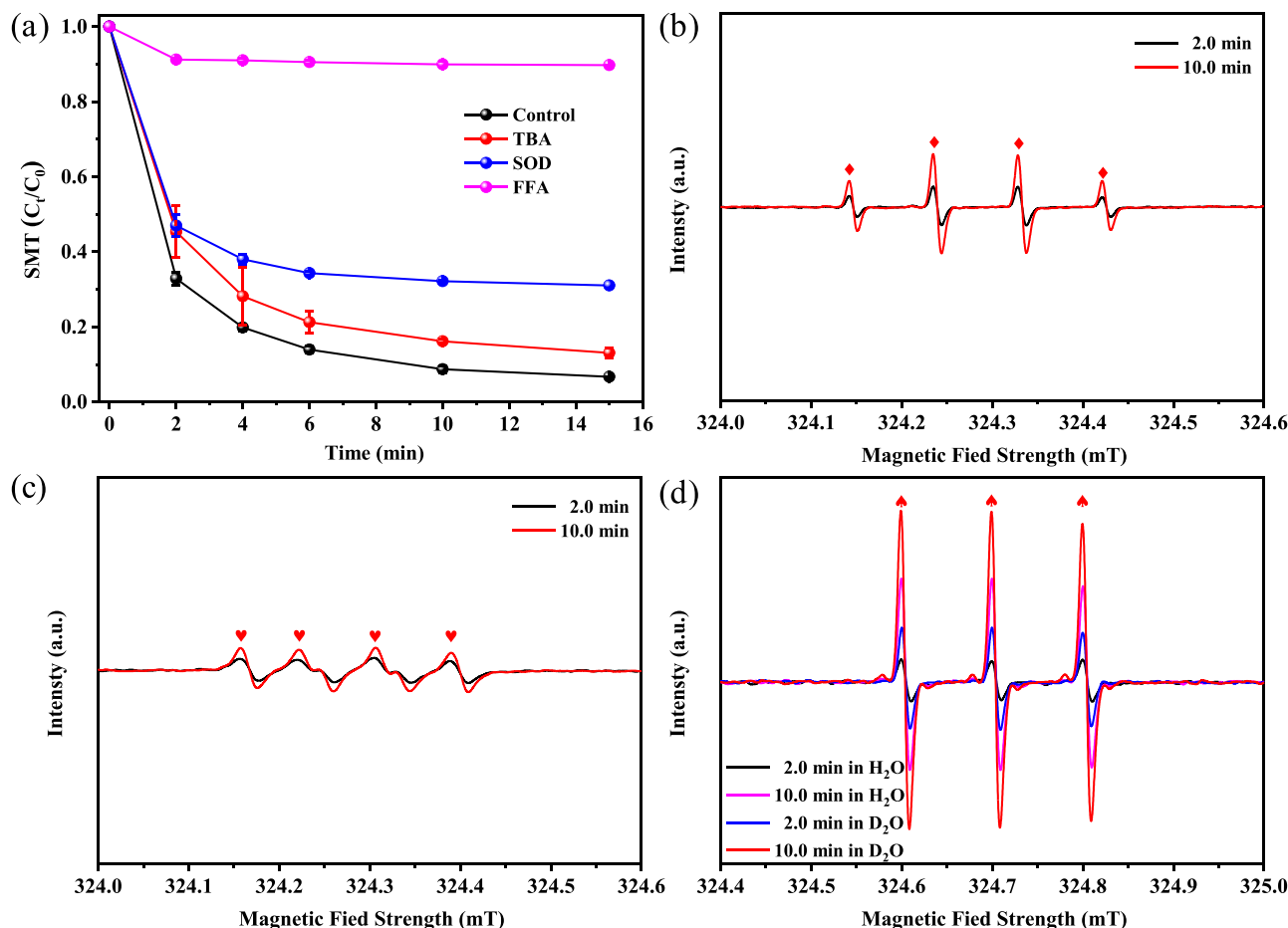
Fig. 2. (a) Effect of TBA, SOD, and FFA on the degradation of SMT. ESR spectrum of (b) DMPO-$^{\bullet}$OH ($\blacklozenge$), (c) DMPO-$O_2^{\bullet-}$ ($\heartsuit$), and (d) TEMP-$^1O_2$ ($\spadesuit$) adducts. Reaction conditions: $[SMT]_0 = 10.0$ μM, $[A\text{-}mZVI]_0 = 10.0$ mg L^{-1}, $[I^-]_0 = 15.0$ μM, $[H_2O_2]_0 = 15.0$ μM, $[TBA]_0 = 3.0$ mM, $[SOD]_0 = 3.0$ mg L^{-1}, $[FFA]_0 = 5.0$ mM, $[DMPO]_0 = 50.0$ mM (only for b and c), $[TEMP]_0 = 40.0$ mM (only for d), $pH_0 = 7.0 \pm 0.1$, and T $= 25.0 \pm 0.5$ °C.

effect on SMT degradation could be negligible.

$$Fe^{2+} + H_2O_2 \rightarrow H_2O + Fe^{IV}O^{2+} \tag{19}$$

In order to further ascertain the ROS might generated in the A-mZVI/H$_2$O$_2$/I$^-$ process, ESR spectroscopy measurement was performed by making use of 5,5-dimethyl-1-pyrolin-N-oxide (DMPO) and 2,2,6,6-tetramethyl-4-piperidinol (TEMP) as the spin-trapping reagents to directly inspect the generation of ROS. As depicted in Fig. 2(b), the ESR signal exhibited the existence of the DMPO-$^{\bullet}$OH adduct in the A-mZVI/H$_2$O$_2$/I$^-$ system. This phenomenon illustrated that $^{\bullet}$OH was indeed formed in the process, which was consistent with the result of quenching experiment by TBA. Similarly, the ESR signal of DMPO-$O_2^{\bullet-}$ was also detected in the A-mZVI/H$_2$O$_2$/I$^-$ system (Fig. 2(c)), which was unanimous with the inhibition of SMT degradation caused by SOD in the quenching experiment. Nevertheless, previous studies have pointed out that the redox potential of $O_2^{\bullet-}$ was exceedingly low ($E^0 = -0.33$ V), and it was theoretically tough to directly eliminate SMT [48]. Therefore, the produced $O_2^{\bullet-}$ was not a momentous species for direct SMT degradation, but rather a crucial precursor for the formation of other ROS (i.e., $^1O_2$) (Eqs. (13–18)). Notably, a strong ESR signal of TEMP-$^1O_2$ was observed in A-mZVI/H$_2$O$_2$/I$^-$ process (Fig. 2(d)), corresponding to the strong suppression of SMT removal by FFA in the quenching experiment. Considering the high-rate constant of physical quenching of $^1O_2$ with H$_2$O ($k = 2.5 \times 10^5$ s^{-1}) and the short lifetime of $^1O_2$ (2.9–4.6 μs) in H$_2$O, deuterium oxide (D$_2$O) was utilized to replace H$_2$O to extend the lifetime of $^1O_2$ (22–70 μs) to further confirm the contribution of $^1O_2$ on SMT removal in the A-mZVI/H$_2$O$_2$/I$^-$ system [49,50]. It can be revealed

that the signal of TEMP-$^1O_2$ captured in D$_2$O was significantly stronger than that trapped in H$_2$O (Fig. 2(d)). Moreover, the peak of TEMP-$^1O_2$ almost disappeared after adding PhOH and TBA to the A-mZVI/H$_2$O$_2$/I$^-$ system, which further explained the main role of $^1O_2$ in the reaction system for the removal of SMT (Fig. S14). Consequently, it could be concluded that among the ROS generated in the A-mZVI/H$_2$O$_2$/I$^-$ system (i.e., $^{\bullet}$OH, $O_2^{\bullet-}$, and $^1O_2$), $^1O_2$ was the predominant ROS for SMT elimination.

3.3.2. The role of iodide

A series of RIS (e.g., I$^{\bullet}$, $I_2^{\bullet-}$, I_3^-, IO_3^-, and HOI) may also exist in the activation system when I$^-$ existed (Eqs. (4–5 and 20–28)) [21,39]. I$^{\bullet}$ might be generated during the reaction of $^{\bullet}$OH with I$^-$/I$_2$ in the A-mZVI/H$_2$O$_2$/I$^-$ system, but was rapidly converted to produce $I_2^{\bullet-}$, and finally back to I$^-$ (Eqs. (4–5 and 26–28)). The change in absorption spectra of I_3^- at 352 nm was monitored by an UV-Vis spectrophotometer (not shown) [24]. Besides, I$_2$ and I_3^- were also not detected in the A-mZVI/H$_2$O$_2$/I$^-$ system using the starch colorimetric method (Fig. S15) [51]. Previously, Bancroft and Murphy reported that IO_3^- can be reduced to I$^-$ by H$_2$O$_2$ when pH was greater than approximately 1.2–1.4, and I$^-$ can be oxidized to IO_3^- by H$_2$O$_2$ when the pH was less than that [52]. Hence, IO_3^- could not be formed via the oxidation of I$^-$ by H$_2$O$_2$ in the A-mZVI/H$_2$O$_2$/I$^-$ process because the pH of the reaction system was about 7.0 (Eq. (29)) [39]. During the water treatment or in natural environment, HOI was the dominant species compared to other iodine species because the concentration of I$^-$ was ordinarily very low [25]. Hence, HOI might be formed in the A-mZVI/H$_2$O$_2$/I$^-$ process. Phenol (PhOH), a potential scavenger of HOI to form o-iodophenol and

p-iodophenol, was used to evaluate the contribution of HOI in the system [24,39]. As observed from Fig. S16, PhOH had a remarkable inhibited influence on the elimination of SMT with the k_{obs} decreased from 0.1622 to 0.0037 min^{-1}. This result suggested that the HOI factually existed in the A-mZVI/H_2O_2/I$^-$ process. Moreover, the HPLC spectra of the A-mZVI/H_2O_2/I$^-$ system in the presence of PhOH were collected, the formation of o-iodophenol and/or p-iodophenol was observed, and the intensity of the peaks increased with reaction time, which further indicated the formation of HOI in the A-mZVI/H_2O_2/I$^-$ system (Fig. S17) [51]. In addition, in order to further explore the function of HOI in the A-mZVI/H_2O_2/I$^-$ system for the degradation of SMT, the signal of TEMP-$^1O_2$ was detected by ESR test after adding PhOH to the A-mZVI/H_2O_2/I$^-$ system (The HOI was consumed by PhOH), and it was found that the intensity of the TEMP-$^1O_2$ was greatly reduced (Fig. S18). This suggested that $^1O_2$ could be formed simultaneously with the reduction of HOI to I$^-$ by H_2O_2, which was consistent with previous report [40].

Preliminarily, the significant enhancement of the degradation of SMT with A-mZVI/H_2O_2 system upon the addtion of I$^-$ indicates that I$^-$ might act as a promising electron shuttle in A-mZVI/H_2O_2/I$^-$ system by accelerating the generation of ROS to remove SMT (Eqs. (4–6 and 20–28)) [39]. The concentration of I$^-$ was virtually unchanged (Fig. S19) during the reaction of 15 min for SMT removal, while H_2O_2 was consumed (Fig. S7). This phenomenon was well explained by the reaction of H_2O_2 with HOI, where HOI was reduced back to I$^-$ with a fast reaction rate ($k_{H2O2/HOI} = 9.8 \times 10^3$ M^{-1} s^{-1}) [53]. Moreover, the solutions of different reaction systems were scanned by an UV–vis spectrophotometer after the reaction of 15 min, and it was found that there was no characteristic peak belonging to other iodine species except for the characteristic peak belonging to I$^-$ at 226 nm (Fig. S20). Hence, I$^-$ might act similarly as the electron shuttle in the A-mZVI/H_2O_2/I$^-$ system for the enhancement of SMT removal.

$$2I^- + H_2O_2 + 2H^+ \rightarrow H_2O + I_2 \tag{20}$$

$$I_2 + H_2O \rightarrow I^- + HOI + H^+ \tag{21}$$

$$I^- + H_2O + H^+ \rightarrow H_2O + HOI \tag{22}$$

$$^\bullet OH + I^- \rightarrow HOI^{\bullet-} \tag{23}$$

$$HOI^{\bullet-} \rightarrow I^\bullet + OH^- \tag{24}$$

$$^\bullet OH + I_2 \rightarrow I^\bullet + HOI \tag{25}$$

$$I^\bullet + I^- \rightarrow I_2^{\bullet-} \tag{26}$$

$$I_2^{\bullet-} + I_2^{\bullet-} \rightarrow I_3^- + I^- \tag{27}$$

$$I_3^- \rightarrow I_2 + I^- \tag{28}$$

$$3HOI \rightarrow IO_3^- + 2I^- + 3H^+ \tag{29}$$

3.3.3. The DFT calculation and determination of intermediates

In order to elucidate the active sites and the pathway of SMT degradation in the A-mZVI/H_2O_2/I$^-$ system, DFT analysis and LC-MS were conducted. The corresponding LC-MS results of SMT were shown in Fig. S21, and the detailed information about the intermediates were listed in Table S3. Fukui index was an important method to evaluate the reaction sites of pollutants. The optimized molecular structure of SMT, the Fukui index isosurface (f^-, f^+, f^0, and Δf), and the condensed Fukui index and dual distribution on SMT were presented in Fig. 3 and Table S4. Theoretically, f^-, f^+, and f^0 represent electrophilic, nucleophilic, and radical attacks, respectively, and atoms on pollutants with high f^-, f^+, and f^0 values are vulnerable to being attacked by electrophilic, nucleophilic, and radical species, respectively [54]. For the highest-energy occupied molecular orbital (HOMO) and the lowest-energy unoccupied molecular orbital (LUMO) of SMT, SMT structurally exhibited a larger distribution density on the benzene and pyrimidine ring moieties (Fig. S22). This result was consistent with the information from the isosurface maps, which indicated that the reactivity of pyrimidine and benzene rings on SMT was higher than that of
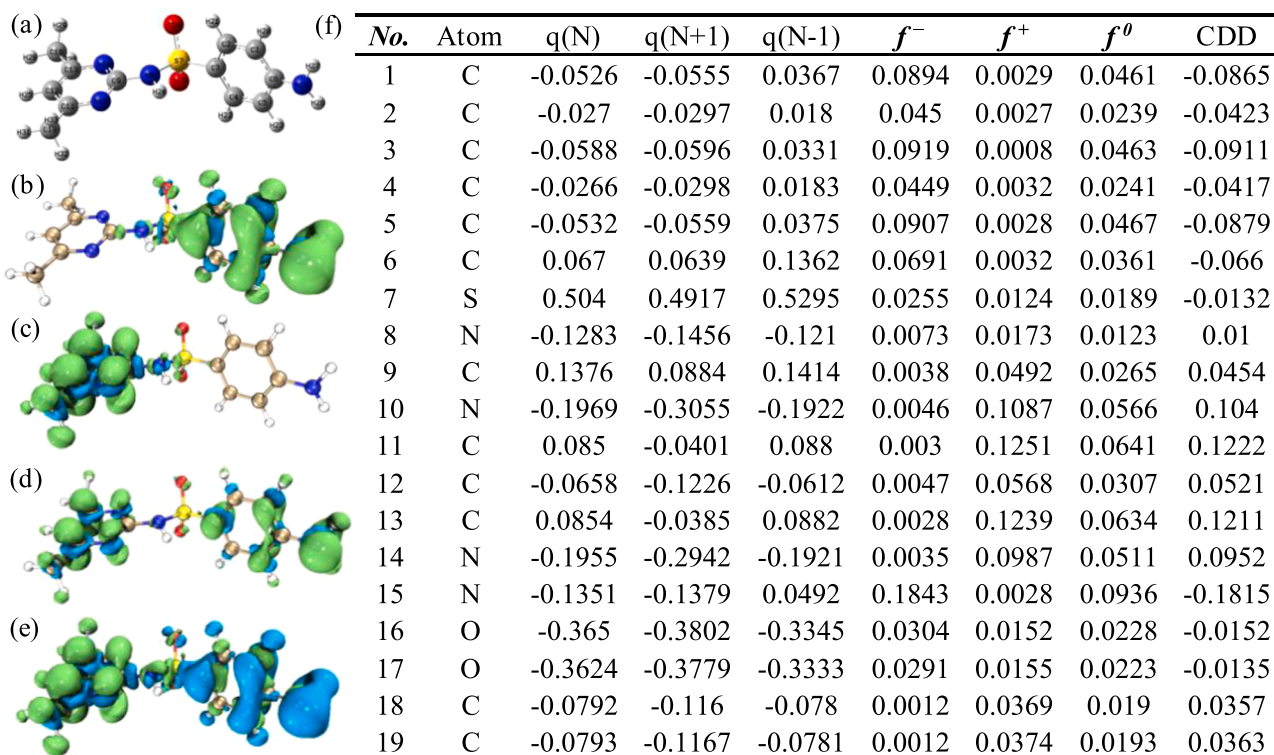

No.	Atom	q(N)	q(N+1)	q(N-1)	f^-	f^+	f^0	CDD
1	C	-0.0526	-0.0555	0.0367	0.0894	0.0029	0.0461	-0.0865
2	C	-0.027	-0.0297	0.018	0.045	0.0027	0.0239	-0.0423
3	C	-0.0588	-0.0596	0.0331	0.0919	0.0008	0.0463	-0.0911
4	C	-0.0266	-0.0298	0.0183	0.0449	0.0032	0.0241	-0.0417
5	C	-0.0532	-0.0559	0.0375	0.0907	0.0028	0.0467	-0.0879
6	C	0.067	0.0639	0.1362	0.0691	0.0032	0.0361	-0.066
7	S	0.504	0.4917	0.5295	0.0255	0.0124	0.0189	-0.0132
8	N	-0.1283	-0.1456	-0.121	0.0073	0.0173	0.0123	0.01
9	C	0.1376	0.0884	0.1414	0.0038	0.0492	0.0265	0.0454
10	N	-0.1969	-0.3055	-0.1922	0.0046	0.1087	0.0566	0.104
11	C	0.085	-0.0401	0.088	0.003	0.1251	0.0641	0.1222
12	C	-0.0658	-0.1226	-0.0612	0.0047	0.0568	0.0307	0.0521
13	C	0.0854	-0.0385	0.0882	0.0028	0.1239	0.0634	0.1211
14	N	-0.1955	-0.2942	-0.1921	0.0035	0.0987	0.0511	0.0952
15	N	-0.1351	-0.1379	0.0492	0.1843	0.0028	0.0936	-0.1815
16	O	-0.365	-0.3802	-0.3345	0.0304	0.0152	0.0228	-0.0152
17	O	-0.3624	-0.3779	-0.3333	0.0291	0.0155	0.0223	-0.0135
18	C	-0.0792	-0.116	-0.078	0.0012	0.0369	0.019	0.0357
19	C	-0.0793	-0.1167	-0.0781	0.0012	0.0374	0.0193	0.0363

Fig. 3. (a) The optimized molecular structure of SMT; The isosurface of Fukui index: (b) f$^-$, (c)f$^+$, (d)f^0, and (e) Δf (The green and blue surfaces correspond to positive and negative regions, respectively); and (f) condensed Fukui index and dual distribution on SMT.

sulfamide group, and the reaction was more likely to occur at these sites. In addition, the Wiberg bond order is an important index to assess the bond strength and bond cleavage [55]. For the same type of chemical bonds, the smaller the Wiberg bond order value, the more likely of the chemical bond was to break. [56]. The Wiberg bond orders in the skeleton of SMT molecule was described in Fig. S23, and the results showed that the S7-N8 bond and S7-C3 bond on the sulfamide group had the smallest bond orders (0.771 and 0.880 for S7-N8 bond and S7-C3 bond, respectively), which indicated that the breakage was most likely to arises at S7-N8 bond and S7-C3 bond.

According to the above DFT theoretical calculation and the detection results of SMT degradation intermediates by LC-MS, the possible degradation pathway of SMT in the A-mZVI/H_2O_2/I^- system was proposed, and the results were shown in Scheme 1. The intermediate P1 (N^1-(4,6-dimethylpyrimidin-2-yl)benzene-1,4-diamine, *m/z* 215) generated by SO_2 extrusion could be attributed to the lower values of Wiberg bond orders at S7-N8 bond and S7-C3 bond. Subsequently, the cleaving of C-N bond and further oxidation occurred to yield the intermediates P2 (2-(hydroxyamino)pyrimidine-4,6-dicarboxylic acid, *m/z* 200) and P3 (2,4,6-trimethylpyrimidine, *m/z* 123). The DFT calculation results showed that the f^0 values of N10, C11, C13 and N14 atoms in the pyrimidine ring were 0.0644, 0.581 and 0.0579, respectively, which were higher than the f^0 values of other atoms, indicating that they were highly vulnerable to $^1O_2$, $O_2^{\bullet-}$ and $^{\bullet}OH$ attack [57]. Hence, the intermediate of P1–1 (4-amino-*N*-carbamimidoylbenzenesulfonamide, *m/z* 215) was obtained by opening ring reaction through radical attack on the reactive site on the pyrimidine ring. Then, the amino group after ring opening was attacked by ROS, resulting in intermediate P4 (2-amino-2-((4-aminophenyl)sulfonamido)acetic acid, *m/z* 246). Later, the amino group located on the benzene ring (f^- was 0.1843) was subjected to electrophilic attack and the S-N bond was also cleaved to yield intermediate P5 (hydrosulfonylbenzene, *m/z* 143). Finally, some smaller molecular weight intermediates (e.g., P6 (hydroquinone, *m/z* 111), P7 (phenol, *m/z* 95), P8 (butane-1,4-diol, *m/z* 91), and P9 ((Z)− 4-aminobut-2-enoic acid, *m/z* 102)), even H_2O and CO_2 were formed owing to the continuous attack by ROS.

3.3.4. Toxicity assessment

To evaluate the potential risks of SMT and its degradation intermediates, QSAR analysis was carried out by the ECOSAR program and T.E.S.T. software [31,32]. The acute and chronic toxicity of SMT and its intermediates for fish, daphnid, and green algae were displayed in Fig. 4 and Table S5. The acute and chronic toxicity of the other intermediates was all lower than that of SMT except for intermediate P1, and most of

them were harmless to the fish, daphnid, and green algae. This prediction was consistent with the results estimated via T.E.S.T on the mutagenicity of SMT and its intermediates, all of them were mutagenicity negative except P1 (Fig. S24). These results suggested that toxicity may be improved or reduced after the elimination of SMT with A-mZVI/H_2O_2/I^- process, but there were still individual intermediates that were more toxic than SMT and needed further attention.

3.3.5. The proposed reaction mechanism for SMT elimination

The surface properties of A-mZVI were characterized by XPS before and after the catalytic reaction. As shown in Fig. 5(a), the XPS spectrum of the Fe 2p range of the fresh A-mZVI showed five major characteristic peaks, the peak of binding energy at 706.9 eV was assigned to Fe^0, the peaks at 710.5 and 724.3 eV corresponded to Fe^{2+} species, and the peaks at 712.8 and 719.5 eV were attributed to Fe^{3+} species [19,35,58]. The appearance of Fe^{2+} and Fe^{3+} peaks indicated that a thin layer of iron (oxy) hydroxide was inevitably wrapped around the iron core (Fe^0) during the preparation of A-mZVI. Compared to fresh A-mZVI, the peaks of Fe^0 and Fe^{2+} species were attenuated after the reaction, and the peaks belonging to the Fe^{3+} species were intensified obviously (Fig. 5(b)). This phenomenon indicated that A-mZVI was oxidized due to the continuous transfer of electrons from the iron core during the catalytic reaction. In addition, the XPS spectrum of O 1 s of A-mZVI before and after use was displayed in Fig. 5(c-d). The two fitted peaks of O 1 s of the fresh A-mZVI at 530.5 and 531.3 eV could be assigned to the Fe-O and -OH, respectively [4,59]. For the used catalyst, the content of surface -OH group decreased, and a new lattice oxygen peak (Fe-O) at 529.7 eV was observed, in addition to an increase in the intensity of Fe-O at 530.5 eV, indicating that oxidation occurred on the A-mZVI surface [4].

Based on the above experimental results and literature reports, the conceivable reaction mechanism for SMT elimination in A-mZVI/H_2O_2/I^- process was proposed. The proposed reaction mechanisms of SMT elimination and involved possible reactions in the A-mZVI/H_2O_2/I^- system were denoted in the Scheme 2 and Table S6. Firstly, A-mZVI released Fe^{2+} from the iron core to the surface by electron transfer (Eqs. (S3-S4)) [12]. Then, H_2O_2 was activated by Fe^{2+} to produce $^{\bullet}OH$ and trace $Fe^{IV}O^{2+}$, and HOI was produced through a series of chain reactions in the existence of I^-. The $O_2^{\bullet-}$ as a precursor for the generation of $^1O_2$ was also generated during this period (Eqs. (S5-S18)) [6,39]. Subsequently, HOI was reduced to I^- in the presence of H_2O_2, and a large amount of $^1O_2$ was also formed in this process. At the same time, other pathways also produced a lot of $^1O_2$ (Eqs. (S19-S25)) [40,43]. Eventually, SMT was degraded by $^1O_2$ and other free radicals.
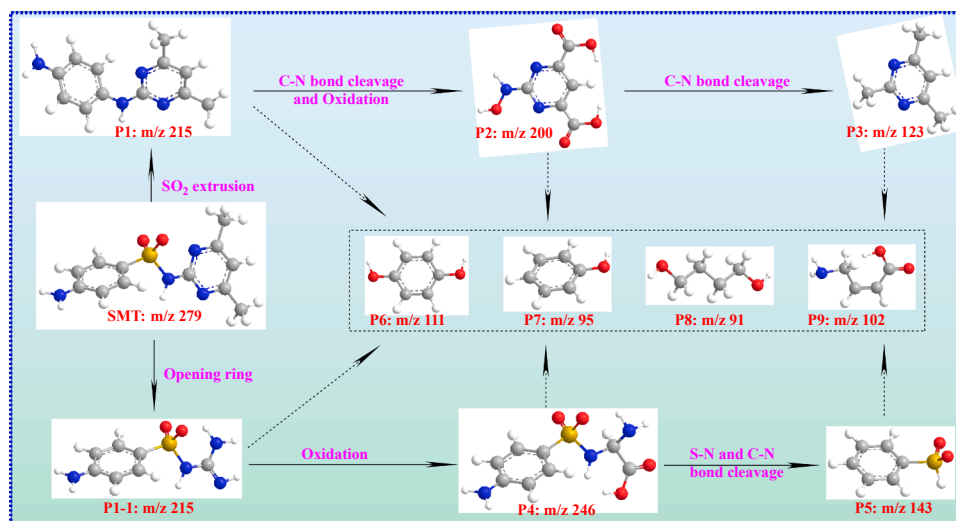
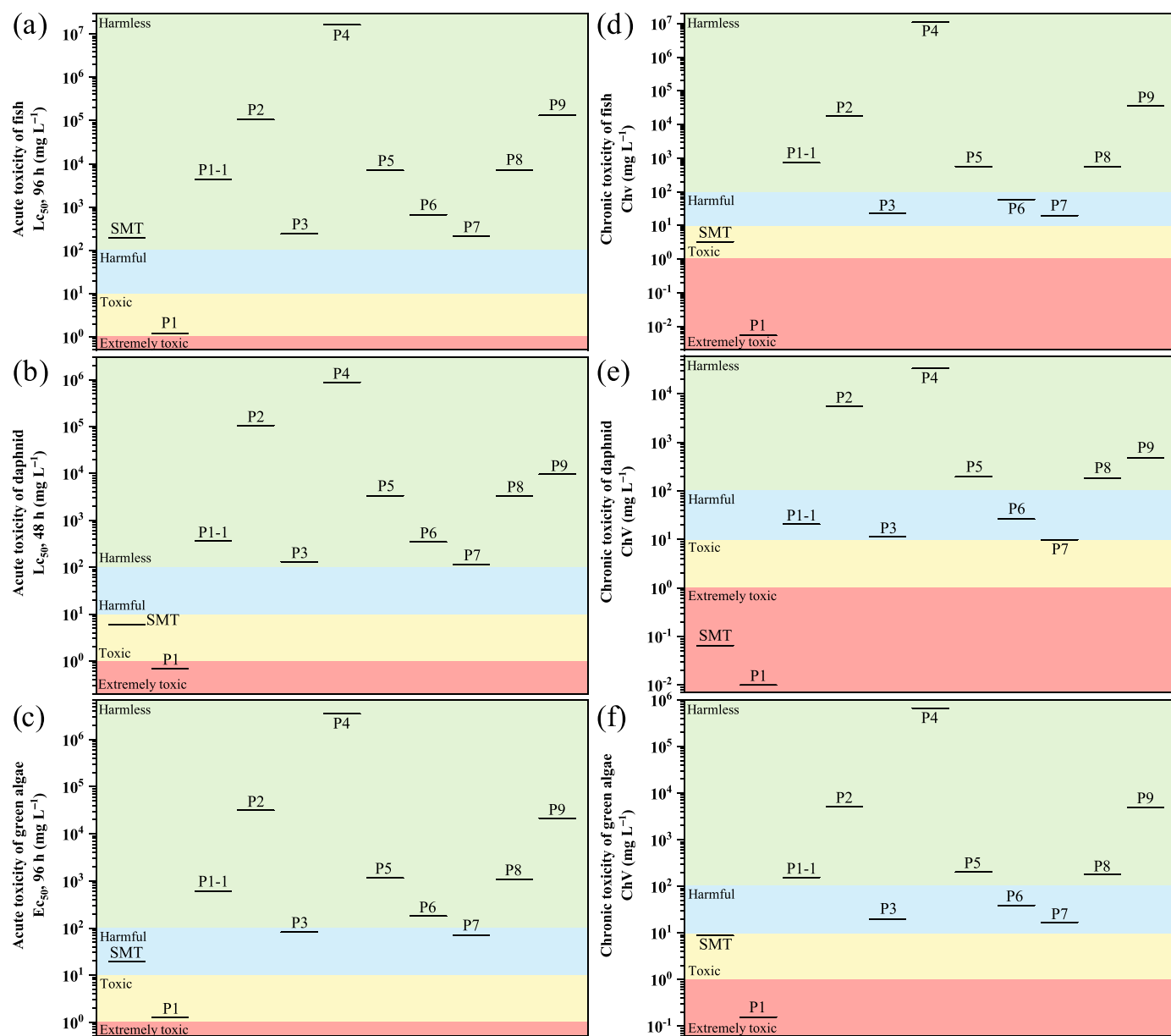**Scheme 1.** The possible degradation pathways of SMT in the A-mZVI/H_2O_2/I^- system.

Fig. 4. (a-c) Acute and (d-f) chronic toxicity of SMT and its intermediates for fish, daphnid, and green algae.

3.4. Effect of key factors on SMT removal

3.4.1. Effect of A-mZVI dosage, H_2O_2 and I^- concentration on SMT removal

For the heterogeneous reaction system, the effect of catalyst dosage on the oxidative system was generally very important, thus the effect of A-mZVI dosage was investigated from 0 to 50.0 mg L^{-1}, and the result was illustrated in Fig. 6**(a)**. Initially, the removal efficiency of SMT increased from 6.1% to 93.3% as the A-mZVI dosage was increased from 0 to 10.0 mg L^{-1}, but when the dosage was further increased to 50.0 mg L^{-1}, the SMT removal efficiency decreased to 38.5%. The reason for this phenomenon may be that primarily increasing the dosage of A-mZVI enables more Fe^{2+} to activate H_2O_2, thereby increasing the removal of SMT. When the dosage of A-mZVI was further increased, Fe^{2+} produced by the catalyst could quench the free radicals and compete with SMT for free radicals (Eq. (30)) [19]. Hence, the dosage of A-mZVI at 10.0 mg L^{-1} was selected for SMT degradation in this study.

$$Fe^{2+} + {}^{\bullet}OH \rightarrow Fe^{3+} + OH^- \tag{30}$$

The concentration of oxidant was also extremely important for AOPs to degrade pollutants, and the concentration of H_2O_2 in the A-mZVI/H_2O_2/I^- system was studied (Fig. 6(b)). As the concentration of H_2O_2 increased from 5.0 μM to 15.0 μM, the removal efficiency of SMT increased significantly from 35.4% to 93.9%. However, when the concentration of H_2O_2 increased to 30.0 μM, the promotion of SMT degradation was quite feeble. Because sufficient H_2O_2 could not only generate more ROS, but also effectively reduce HOI to I^-. Therefore, based on the effect of H_2O_2 concentration on SMT degradation and reduction of HOI, as well as economic issues, a concentration of 15.0 μM H_2O_2 was chosen for SMT degradation in the present study.

The influence of the concentration of I^- on the SMT elimination was also investigated by examining various doses of I^- from 0 to 100.0 μM. As observed in Fig. 6**(c)**, the removal efficiency of SMT improved from 12.4% to 93.3% with the I^- concentration promoted from 0 to 15.0 μM during the reaction of 15 min. Nevertheless, overdose of I^- (50.0–100.0 μM) strongly inhibited the elimination of SMT in the A-mZVI/H_2O_2/I^- system. This phenomenon indicated that there was also an optimum I^- concentration for SMT elimination in the A-mZVI/H_2O_2/
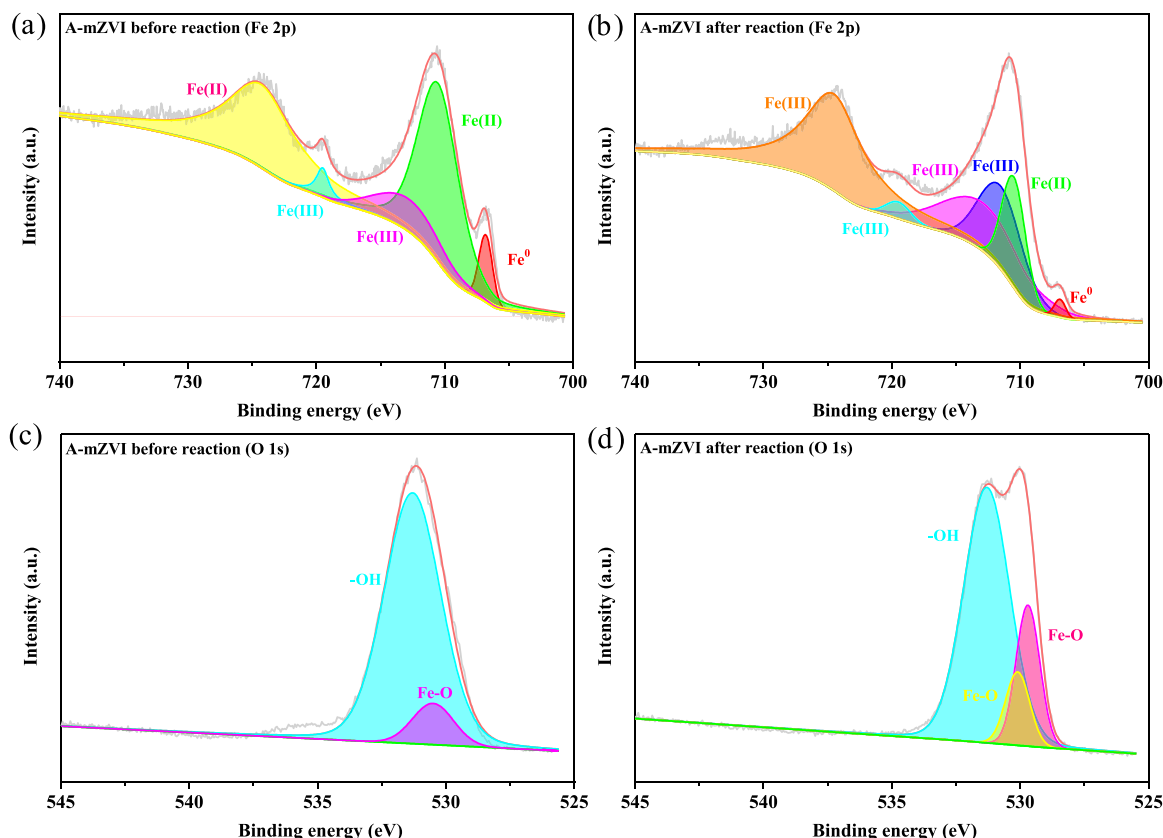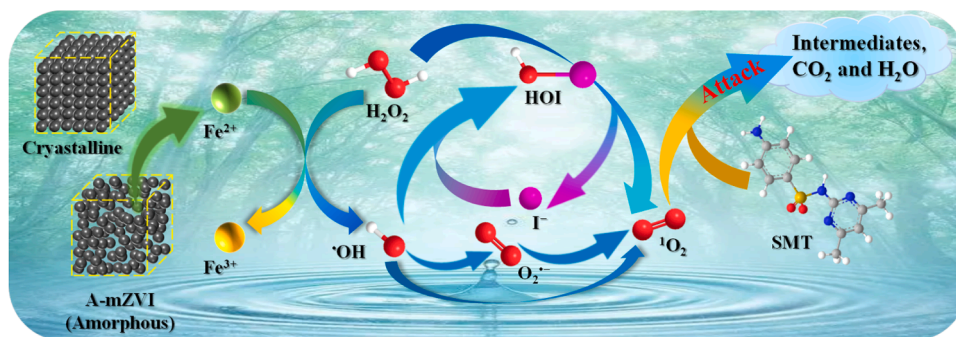
Fig. 5. XPS spectra of Fe 2p and O 1 s of A-mZVI before (a and c) and after (b and d) reaction.

**Scheme 2.** The proposed mechanisms of SMT elimination in A-mZVI/H_2O_2/I^- system.

I^- process. Accordingly, 15.0 μM was chosen as the optimal concentration of I^- to remove SMT in the A-mZVI/H_2O_2/I^- system at the present study.

3.4.2. Effect of initial pH on SMT removal

The pH could not only affect the surface charge of materials, but also affect the existence form of substances, thereby it was necessary to investigate the influence of solution pH on the SMT degradation in the A-mZVI/H_2O_2/I^- system. As illustrated in Fig. 6(d), the removal efficiency of SMT was less than 25.0% and 15.0% at the initial solution pH values of 3.0 and 9.0 after 15 min, respectively. The removal of SMT in the absence of I^- at pH 3.0 was also studied, and the results was shown in Fig. S25. It was demonstrated that the removal efficiency of SMT in the absence of I^- was basically the same as that in the presence of I^-. This phenomenon revealed that the addition of I^- did not act as an electron shuttle to enhance the degradation of SMT in the strong acidic condition (pH 3.0). The reasons for the inferior removal efficiency of SMT under

strong alkaline conditions may be the following reasons. Firstly, the Zeta potential of A-mZVI was measured, and the result was shown in Fig. S26. The zero point charge of A-mZVI was found at pH of 6.9. When the pH value is less than 6.9, the surface of the material is positively charged, and vice versa. Additionally, the species distribution of SMT at different pH values was also investigated. As illustrated in Fig. S27, SMT exists mainly in the deprotonated form (SMT^-) at pH 9.0. Therefore, it may be due to the negative charge on the surface of A-mZVI at pH 9.0, while SMT mainly behaves as SMT^-, and the degradation of SMT on the reactive site of A-mZVI was hindered due to the electrostatic repulsion. On the other hand, it was possible that the reaction rate between I^- and H_2O_2 decreased under strongly alkaline condition. This phenomenon also occurred in the removal of phenolic pollutants in the PMS/I^- system [27]. In addition, Lente et al. investigated the oxidation kinetics of I^- in PMS solutions and found that the rate constant decreased sharply when the solution pH was above 8.0 [60]. Accordingly, it was found that A-mZVI/H_2O_2/I^- system achieved its optimum degradation capability
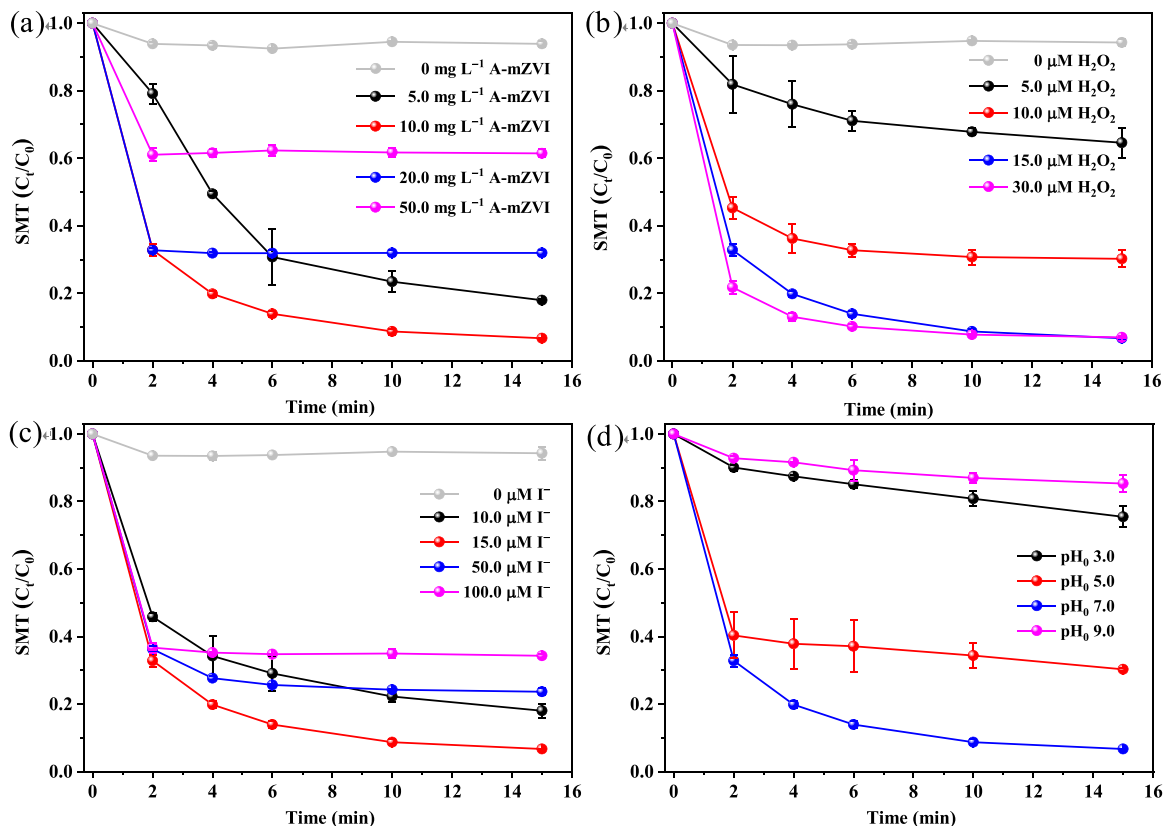
Fig. 6. Effect of (a) A-mZVI dosage, (b) H_2O_2 concentration, (c) I^- concentration, and (d) initial pH on the degradation of SMT in the A-mZVI/H_2O_2/I^- system. Reaction conditions: $[SMT]_0 = 10.0\ \mu M$, $[A\text{-}mZVI]_0 = 10.0\ mg\ L^{-1}$, $[I^-]_0 = 15.0\ \mu M$, $[H_2O_2]_0 = 15.0\ \mu M$, $pH_0 = 7.0 \pm 0.1$, and $T = 25.0 \pm 0.5\ °C$.
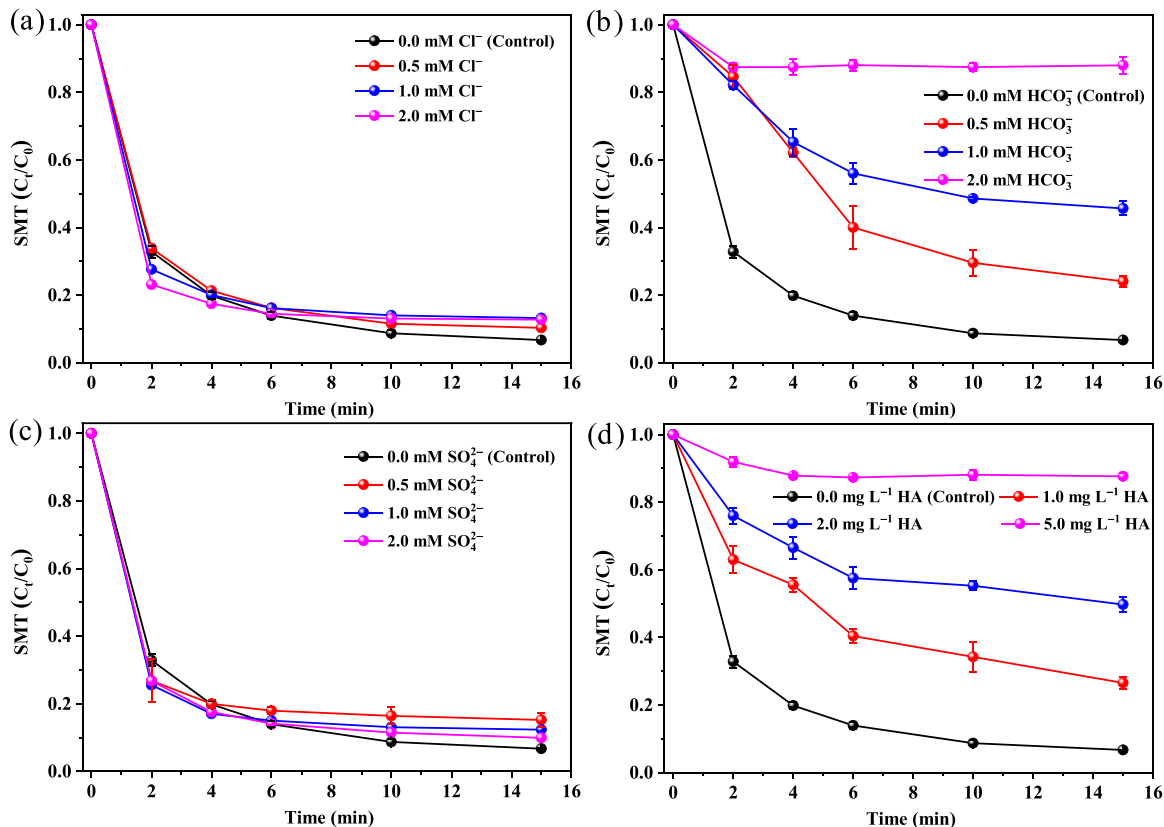
Fig. 7. Effect of the concentration of (a) Cl^-, (b) HCO_3^-, (c) SO_4^{2-}, and (d) humic acid on the degradation of SMT in the A-mZVI/H_2O_2/I^- system. Reaction conditions: $[SMT]_0 = 10.0\ \mu M$, $[A\text{-}mZVI]_0 = 10.0\ mg\ L^{-1}$, $[I^-]_0 = 15.0\ \mu M$, $[H_2O_2]_0 = 15.0\ \mu M$, $pH_0 = 7.0 \pm 0.1$, and $T = 25.0 \pm 0.5\ °C$.

for SMT around neutral condition, indicating that no additional pH adjustment is required before treatment of actual water bodies (usually at circumneutral pH). This represented a major advantage over the classical Fenton process, which only worked effectively under strongly acidic condition around 3.0, and may require a pH adjustment step prior to treatment for actual water matrix.

3.4.3. Effect of inorganic anions and humic acid on SMT removal

To evaluate the anti-interference capacity of the A-mZVI/H_2O_2/I^- system, the effect of the common inorganic anions (i.e., Cl^-, HCO_3^-, SO_4^{2-}) and humic acid (HA) that commonly existed in natural water environment on SMT degradation was investigated. As depicted in Fig. 7, it could be discovered that Cl^- and SO_4^{2-} had a negligible influence on the removal of SMT in the A-mZVI/H_2O_2/I^- process. Nevertheless, HCO_3^- and HA had a significant influence on the degradation of SMT in A-mZVI/H_2O_2/I^- system. With the increase of HCO_3^- concentrations, the inhibition of SMT degradation was more obvious, which may be due to the fact that $^\bullet OH$ could be scavenged by HCO_3^- to generate relatively less reactive $CO_3^{\bullet-}$ (Eq. (31)) [31]. There were three possible reasons for the inhibitory effect of HA on the removal of SMT in the A-mZVI/H_2O_2/I^- system. One was that the phenolic hydroxyl and carboxyl groups of HA could blocked the catalytic site of A-mZVI, thus hindering the activation of H_2O_2 [43,61]; one was that the phenolic substances that existed in HA could react with the key intermediate substance HOI [29]; the other was that with the excess HA added, it consumed H_2O_2 and quenched $^1O_2$ in large quantities, inhibiting the oxidation of SMT [62].

$$HCO_3^- + {}^\bullet OH \rightarrow CO_3^{\bullet-} + H_2O \tag{31}$$

3.5. Practicability evaluation

To explore the application prospects of the A-mZVI/H_2O_2/I^- process, the SMT removal by the A-mZVI/H_2O_2/I^- system in two actual water matrix (i.e., groundwater and river water) was further conducted. As illustrated in Fig. S28(a), the degradation of SMT was repressed to a different extent in the natural water matrix, but the removal efficiency of SMT was still above 70.0% within 15 min. This result suggested that the proposed A-mZVI/H_2O_2/I^- process could still be a promising highly-efficient process in removing micropollutants in actual water matrix. Nevertheless, it should be remarked that the removal efficiency of SMT decreased from 93.3% in ultrapure water to 70.1% in river water in the reaction of 15 min, and the corresponding k_{obs} decreased from 0.3209 min^{-1} to 0.1632 min^{-1} in the first 6 min of reaction (Fig. S28 (b)). The river water sample usually contained abundant natural organic matter (NOM), and it could be rational to infer that the inhibition of SMT degradation in the natural water matrix was mainly owing to the influence of coexistent NOM [63].

In addition, three other micropollutants including sulfadiazine (SDZ), bisphenol A (BPA), and acetaminophen (ACE) were selected to further evaluate the applicability of A-mZVI/H_2O_2/I^- process, and the results could be seen in Fig. S29. It was revealed that the A-mZVI/H_2O_2/I^- process had an outstanding oxidation performance on SMT, SDZ, and BPA with the removal efficiencies of 93.3%, 97.7%, and 94.2%, respectively, and the corresponding k_{obs} values were 0.1622, 0.2015, and 0.1984 min^{-1}. However, the removal efficiency of ACE was only 61.4% within 15 min. The selective oxidation of different micropollutants in the A-mZVI/H_2O_2/I^- system could be ascribed to the high selectivity of ROS [64]. Furthermore, the reusability of A-mZVI was investigated in the A-mZVI/H_2O_2/I^- system (Fig. S30). The removal efficiency of SMT was decreased to a certain extent after three cycles, but still maintained at about 70.0%, indicating that A-mZVI exhibited a favorable reusability in the A-mZVI/H_2O_2/I^- system at neutral pH.

4. Conclusions

In this study, I^- was applied as an electron shuttle to significantly accelerate the elimination of SMT with H_2O_2 activated by A-mZVI under neutral condition. Under optimal reaction conditions (i.e., 15.0 μM H_2O_2, 15.0 μM I^-, and 10.0 mg L^{-1} A-mZVI, and at initial pH of 7.0), SMT could be degraded efficiently within 15 min (93.3%). Multiple reactive species including $^\bullet OH$, $O_2^{\bullet-}$, $Fe^{IV}O^{2+}$, $^1O_2$, and HOI were detected in A-mZVI/H_2O_2/I^- system via quenching experiments, PMSO-based probe experiment, and ESR tests, and $^1O_2$ was the predominant reactive species for SMT elimination. The mechanism for the enhanced performance in the A-mZVI/H_2O_2/I^- system was proposed, and the degradation pathway of SMT was inferred via DFT calculation and the determined intermediate products. The toxicity assessment of the intermediates was also conducted via the QSAR method, and the acute and chronic toxicity of most intermediates was all lower than that of SMT except for a few intermediates. The common inorganic anions like Cl^- and SO_4^{2-} showed negligible impacts on SMT removal, but SMT elimination was inhibited in the presence of HCO_3^- and HA. The proposed A-mZVI/H_2O_2/I^- system exhibited a selectivity towards different micropollutants and was efficient to remove SMT in the natural water matrix. Furthermore, A-mZVI still exhibited a favorable reusability in the A-mZVI/H_2O_2/I^- system after three cycles at neutral pH. In summary, the proposed A-mZVI/H_2O_2/I^- process is a promising approach with practical potential of degrading micropollutants in water treatment.

CRediT authorship contribution statement

Zhao Mengxi: Writing – review & editing. **Pang Zijun:** Software, Writing – review & editing. **Dong Haoran:** Conceptualization, Funding acquisition, Supervision, Writing – review & editing. **Li Yangju:** Methodology, Writing – review & editing. **Xiao Junyang:** Investigation, Methodology, Writing – original draft. **Li Long:** Writing – review & editing. **Huang Daofen:** Writing – review & editing. **Dong Jie:** Writing – review & editing.

Declaration of Competing Interest

The authors declare that they have no known competing financial interests or personal relationships that could have appeared to influence the work reported in this paper.

Data Availability

Data will be made available on request.

Acknowledgements

Supporting Information

Additional texts (Text S1-S4), tables (Table S1-S6), and figures (Figs. S1- S30) can be found on line.

Appendix A. Supporting information

Supplementary data associated with this article can be found in the online version at doi:10.1016/j.apcatb.2023.123610.

References

[1] H. Cai, J. Zou, J. Lin, J. Li, Y. Huang, S. Zhang, B. Yuan, J. Ma, Sodium hydroxide-enhanced acetaminophen elimination in heat/peroxymonosulfate system:

production of singlet oxygen and hydroxyl radical, Chem. Eng. J. 429 (2022), 132438.

[2] Y. Jing, M. Jia, Z. Xu, W. Xiong, Z. Yang, H. Peng, J. Cao, Y. Xiang, C. Zhang, Facile synthesis of recyclable 3D gelatin aerogel decorated with MIL-88B(Fe), Act. peroxydisulfate Degrad. norfloxacin, J. Hazard. Mater. 424 (2022), 127503.

[3] Y. Li, H. Dong, L. Li, L. Tang, R. Tian, R. Li, J. Chen, Q. Xie, Z. Jin, J. Xiao, S. Xiao, G. Zeng, Recent advances in waste water treatment through transition metal sulfides-based advanced oxidation processes, Water Res 192 (2021), 116850.

[4] J. Xiao, R. Li, H. Dong, Y. Li, L. Li, S. Xiao, Z. Jin, Activation of sulfite via zero-valent iron-manganese bimetallic nanomaterials for enhanced sulfamethazine removal in aqueous solution: Key roles of Fe/Mn molar ratio and solution pH, Sep. Purif. Technol. 297 (2022), 121479.

[5] L. Wang, J. Jiang, J. Ma, S. Pang, T. Zhang, A review on advanced oxidation processes homogeneously initiated by copper(II), Chem. Eng. J. 427 (2022), 131721.

[6] Y. Liu, Y. Zhao, J. Wang, Fenton/Fenton-like processes with in-situ production of hydrogen peroxide/hydroxyl radical for degradation of emerging contaminants: advances and prospects, J. Hazard. Mater. 404 (2021), 124191.

[7] M. Azfar Shaida, S. Verma, S. Talukdar, N. Kumar, M. Salim Mahtab, M. Naushad, I. Haq Farooqi, Critical analysis of the role of various iron-based heterogeneous catalysts for advanced oxidation processes: a state of the art review, J. Mol. Liq. 374 (2023), 121259.

[8] Y. Segura, F. Martínez, J.A. Melero, Effective pharmaceutical wastewater degradation by Fenton oxidation with zero-valent iron, Appl. Catal. B Environ. 136-137 (2013) 64–69.

[9] H. Luo, Y. Zeng, D. He, X. Pan, Application of iron-based materials in heterogeneous advanced oxidation processes for wastewater treatment: a review, Chem. Eng. J. 407 (2021), 127191.

[10] A. Asghar, A.A. Abdul Raman, W.M.A. Wan Daud, Advanced oxidation processes for in-situ production of hydrogen peroxide/hydroxyl radical for textile wastewater treatment: a review, J. Clean. Prod. 87 (2015) 826–838.

[11] R. Li, H. Dong, R. Tian, J. Chen, Q. Xie, Activation of sulfite by different Fe^0-based nanomaterials for oxidative removal of sulfamethazine in aqueous solution, Sep. Purif. Technol. 250 (2020), 117230.

[12] Y. Han, X. Zhou, L. Lei, H. Sun, Z. Niu, Z. Zhou, Z. Xu, H. Hou, Efficient activation of persulfate by calcium sulfate whisker supported nanoscale zero-valent iron for methyl orange removal, RSC Adv. 11 (2020) 452–461.

[13] D.H. Bremner, A.E. Burgess, D. Houllemare, K. Namkung, Phenol degradation using hydroxyl radicals generated from zero-valent iron and hydrogen peroxide, Appl. Catal. B Environ. 63 (2006) 15–19.

[14] W. Wang, P. Zhao, Y. Hu, R. Zan, Application of weak magnetic field coupling with zero-valent iron for remediation of groundwater and wastewater: a review, J. Clean. Prod. 262 (2020), 121341.

[15] H. Dong, Z. Jiang, C. Zhang, J. Deng, K. Hou, Y. Cheng, L. Zhang, G. Zeng, Removal of tetracycline by Fe/Ni bimetallic nanoparticles in aqueous solution, J. Colloid Interf. Sci. 513 (2018) 117–125.

[16] J. Chen, H. Dong, R. Tian, R. Li, Q. Xie, Remediation of trichloroethylene-contaminated groundwater by sulfide-modified nanoscale zero-valent iron supported on biochar: investigation of critical factors, Water, Air, Soil Pollut. (231 () (2020).

[17] J. Wu, B. Wang, L. Blaney, G. Peng, P. Chen, Y. Cui, S. Deng, Y. Wang, J. Huang, G. Yu, Degradation of sulfamethazine by persulfate activated with organo-montmorillonite supported nano-zero valent iron, Chem. Eng. J. 361 (2019) 99–108.

[18] Y.B. Hu, M.Y. Zhang, R.L. Qiu, X.Y. Li, Encapsulating nanoscale zero-valent iron with a soluble $Mg(OH)_2$ shell for improved mobility and controlled reactivity release, J. Mater. Chem. A 6 (2018) 2517–2526.

[19] J. Xiao, S. Xiao, H. Dong, Z. Jin, Y. Li, L. Li, R. Tian, R. Li, J. Chen, Q. Xie, Degradation of sulfamethazine by amorphous zero-valent iron microspheres (A-mZVI) activated peroxydisulfate in groundwater, J. Clean. Prod. 346 (2022), 131276.

[20] J. Wang, Z. Shu, Z. Chen, J. Su, C. Liu, Iodide ions enhancing sulfamerazine degradation by horseradish peroxidase/H_2O_2: Degradation products, degradation mechanism and toxicity assessment, J. Clean. Prod. 337 (2022), 130489.

[21] H. MacKeown, U. von Gunten, J. Criquet, Iodide sources in the aquatic environment and its fate during oxidative water treatment – A critical review, Water Res 217 (2022), 118417.

[22] X. Wang, Y. Liu, S. Xu, J. Zhang, J. Li, H. Song, Z. Zhang, L. Wang, J. Ma, Ferrate oxidation of phenolic compounds in iodine-containing water: control of iodinated aromatic products, Environ. Sci. Technol. 54 (2020) 1827–1836.

[23] D.A. House, Kinetics and mechanism of oxidations by peroxydisulfate, Chem. Rev. 62 (1962) 185–203.

[24] J. Li, J. Jiang, Y. Zhou, S. Pang, Y. Gao, C. Jiang, J. Ma, Y. Jin, Y. Yang, G. Liu, L. Wang, C. Guan, Kinetics of Oxidation of Iodide (I^-) and Hypoiodous Acid (HOI) by Peroxymonosulfate (PMS) and Formation of Iodinated Products in the PMS/I^-/NOM System, Environ. Sci. Technol. Lett. 4 (2017) 76–82.

[25] J. Shin, Y. Lee, U. von Gunten, Kinetics of the reaction between hydrogen peroxide and aqueous iodine: Implications for technical and natural aquatic systems, Water Res 179 (2020), 115852.

[26] X. Zhao, E. Salhi, H. Liu, J. Ma, U. von Gunten, Kinetic and mechanistic aspects of the reactions of iodide and hypoiodous acid with permanganate: oxidation and disproportionation, Environ. Sci. Technol. 50 (2016) 4358–4365.

[27] Y. Feng, P. Lee, D. Wu, K. Shih, Rapid selective circumneutral degradation of phenolic pollutants using peroxymonosulfate–iodide metal-free oxidation: role of iodine atoms, Environ. Sci. Technol. 51 (2017) 2312–2320.

[28] J. Li, Y. Zhou, J. Jiang, S. Pang, Y. Gao, Y. Yang, G. Liu, J. Ma, C. Jiang, L. Wang, Transformation of phenolic compounds by peroxymonosulfate in the presence of iodide and formation of iodinated aromatic products, Chem. Eng. J. 335 (2018) 855–864.

[29] J. Li, J. Jiang, S.Y. Pang, Y. Cao, Y. Zhou, C. Guan, Oxidation of iodide and hypoiodous acid by non-chlorinated water treatment oxidants and formation of iodinated organic compounds: a review, Chem. Eng. J. 386 (2020), 123822.

[30] Y. Liu, L. Chen, X. Liu, T. Qian, M. Yao, W. Liu, H. Ji, Tuning band structure of graphitic carbon nitride for efficient degradation of sulfamethazine: atmospheric condition and theoretical calculation, Chinese, Chem. Lett. 33 (2022) 1385–1389.

[31] J. Xiao, H. Dong, Y. Li, L. Li, D. Chu, S. Xiang, X. Hou, Q. Dong, S. Xiao, Z. Jin, J. Wang, Graphene shell-encapsulated copper-based nanoparticles (G@Cu-NPs) effectively activate peracetic acid for elimination of sulfamethazine in water under neutral condition, J. Hazard. Mater. 441 (2023), 129895.

[32] Y. Huang, J. Zou, J. Lin, H. Yang, M. Wang, J. Li, W. Cao, B. Yuan, J. Ma, ABTS as both activator and electron shuttle to activate persulfate for diclofenac degradation: formation and contributions of $ABTS^{\bullet+}$, $SO_4^{\bullet-}$, and $^{\bullet}OH$, Environ. Sci. Technol. (2022), https://doi.org/10.1021/acs.est.2c04318.

[33] W. Shen, X. Wang, F. Jia, Z. Tong, H. Sun, X. Wang, F. Song, Z. Ai, L. Zhang, B. Chai, Amorphization enables highly efficient anaerobic thiamphenicol reduction by zero-valent iron, Appl. Catal. B Environ. 264 (2020), 118550.

[34] H. Sun, J. Wang, Y. Jiang, W. Shen, F. Jia, S. Wang, X. Liao, L. Zhang, Rapid aerobic inactivation and facile removal of escherichia coli with amorphous zero-valent iron microspheres: indispensable roles of reactive oxygen species and iron corrosion products, Environ. Sci. Technol. 53 (2019) 3707–3717.

[35] W. Shen, F. Lin, X. Jiang, H. Li, Z. Ai, L. Zhang, Efficient removal of bromate with core-shell Fe@Fe_2O_3 nanowires, Chem. Eng. J. 308 (2017) 880–888.

[36] Q. Cheng, Q. Li, X. Huang, X. Li, Y. Wang, W. Liu, Z. Lin, The high efficient Sb(III) removal by cauliflower like amorphous nanoscale zero-valent iron (A-nZVI), J. Hazard. Mater. 436 (2022), 129056.

[37] J. Xiao, Y. Li, H. Dong, Z. Pang, M. Zhao, D. Huang, J. Dong, L. Li, Highly efficient activation of peracetic acid via zero-valent iron-copper bimetallic nanoparticles (nZVIC) for the oxidation of sulfamethazine in aqueous solution under neutral condition, Appl. Catal. B Environ. 340 (2024), 123183.

[38] S. Xiang, H. Dong, Y. Li, J. Xiao, Q. Dong, X. Hou, D. Chu, Novel flower-like Fe-Mo composite for peroxydisulfate activation toward efficient degradation of carbamazepine, Sep. Purif. Technol. 305 (2023), 122487.

[39] Z. Chen, J. Li, K.Y. Koh, Z. Du, C.N. Ong, J.P. Chen, Kinetics and mechanism investigation of selective arsenite oxidation by reactive iodine species in hydrogen peroxide and iodide (H_2O_2/I^-) system, ACS ES&T Water 1 (2021) 1515–1523.

[40] J.R. Kanofsky, Singlet oxygen production by chloroperoxidase-hydrogen peroxide-halide systems, J. Biol. Chem. 259 (1984) 5596–5600.

[41] Y. Zhang, M. Zhou, A critical review of the application of chelating agents to enable Fenton and Fenton-like reactions at high pH values, J. Hazard. Mater. 362 (2019) 436–450.

[42] Q. Li, B. Hu, Q. Yang, X. Cai, M. Nie, Y. Jin, L. Zhou, Y. Xu, Q. Pan, L. Fang, Interaction mechanism between multi-layered MoS_2 and H_2O_2 for self-generation of reactive oxygen species, Environ. Res. 191 (2020), 110227.

[43] Y. Li, H. Dong, J. Xiao, L. Li, D. Chu, X. Hou, S. Xiang, Q. Dong, Insights into a novel CuS/percarbonate/tetraacetylethylenediamine process for sulfamethazine degradation in alkaline medium, J. Hazard. Mater. 435 (2022), 128999.

[44] Z. Yang, C. Shan, B. Pan, J.J. Pignatello, The Fenton reaction in water assisted by picolinic acid: accelerated iron cycling and co-generation of a selective Fe-Based oxidant, Environ. Sci. Technol. 55 (2021) 8299–8308.

[45] M. Jiang, J. Lu, Y. Ji, D. Kong, Bicarbonate-activated persulfate oxidation of acetaminophen, Water Res 116 (2017) 324–331.

[46] J. Kim, T. Zhang, W. Liu, P. Du, J.T. Dobson, C. Huang, Advanced oxidation process with peracetic acid and Fe(II) for contaminant degradation, Environ. Sci. Technol. 53 (2019) 13312–13322.

[47] S. Pang, J. Jiang, J. Ma, Oxidation of sulfoxides and arsenic(III) in corrosion of nanoscale zero valent iron by oxygen: evidence against ferryl ions (Fe(IV)) as active intermediates in fenton reaction, Environ. Sci. Technol. 45 (2011) 307–312.

[48] L. Wu, Z. Sun, Y. Zhen, S. Zhu, C. Yang, J. Lu, Y. Tian, D. Zhong, J. Ma, Oxygen VAcancy-induced Nonradical Degradation of Organics: Critical Trigger of Oxygen (O_2) in the Fe–Co LDH/peroxymonosulfate system, Environ. Sci. Technol. 55 (2021) 15400–15411.

[49] B. Liu, W. Guo, W. Jia, H. Wang, S. Zheng, Q. Si, Q. Zhao, H. Luo, J. Jiang, N. Ren, Insights into the oxidation of organic contaminants by Co(II) activated peracetic acid: the overlooked role of high-valent cobalt-oxo species, Water Res 201 (2021), 117313.

[50] S. Zuo, Z. Guan, D. Xia, F. Yang, H. Xu, M. Huang, D. Li, Polarized heterogeneous CuO-CN for peroxymonosulfate nonradical activation: an enhancement mechanism of mediated electron transfer, Chem. Eng. J. 420 (2021), 127619.

[51] Y. Zong, H. Zhang, Y. Shao, W. Ji, Y. Zeng, L. Xu, D. Wu, Surface-mediated periodate activation by nano zero-valent iron for the enhanced abatement of organic contaminants, J. Hazard. Mater. 423 (2022), 126991.

[52] W.D. Bancroft, N.F. Murphy, Oxidation and reduction with hydrogen peroxide, J. Phys. Chem. 39 (1935) 377–398.

[53] G.T.F. Wong, L. Zhang, The kinetics of the reactions between iodide and hydrogen peroxide in seawater, Mar. Chem. 111 (2008) 22–29.

[54] Z. Xie, C. He, D. Pei, Y. Zheng, X. Wu, Z. Xiong, Y. Du, Z. Pan, G. Yao, B. Lai, Efficient degradation of micropollutants in CoCaAl-LDO/peracetic acid (PAA) system: an organic radical dominant degradation process, J. Hazard. Mater. 452 (2023), 131286.

[55] I. Mayer, Bond order and valence indices: a personal account, J. Comput. Chem. 28 (2007) 204–221.

[56] L. Shen, Z. Chen, J. Kang, P. Yan, J. Shen, B. Wang, S. Zhao, L. Bi, S. Wang, Y. Cheng, N-nitrosodimethylamine formation during oxidation of N,N-dimethylhydrazine compounds by peroxymonosulfate: kinetics, reactive species, mechanism and influencing factors, J. Hazard. Mater. 428 (2022), 128191.

[57] S. Li, Y. Yang, H. Zheng, Y. Zheng, C. He, B. Lai, J. Ma, J. Nan, Introduction of oxygen vacancy to manganese ferrite by Co substitution for enhanced peracetic acid activation and $^1O_2$ dominated tetracycline hydrochloride degradation under microwave irradiation, Water Res 225 (2022), 119176.

[58] Q. Dong, H. Dong, Y. Li, J. Xiao, S. Xiang, X. Hou, D. Chu, Degradation of sulfamethazine in water by sulfite activated with zero-valent Fe-Cu, bimetallic Nanopart., J. Hazard. Mater. 431 (2022), 128601.

[59] Y. Yang, L. Xu, W. Li, W. Fan, S. Song, J. Yang, Adsorption and degradation of sulfadiazine over nanoscale zero-valent iron encapsulated in three-dimensional graphene network through oxygen-driven heterogeneous Fenton-like reactions, Appl. Catal. B Environ. 259 (2019), 118057.

[60] G. Lente, J. Kalmár, Z. Baranyai, A. Kun, I. Kék, D. Bajusz, M. Takács, L. Veres, I. Fábián, One- versus two-electron oxidation with peroxomonosulfate ion: reactions with iron(ii), vanadium(iv), halide ions, and photoreaction with cerium (III), Inorg. Chem. 48 (2009) 1763–1773.

[61] Y. Liu, S. Wang, Z. Wang, Y. Fu, R. Zhou, FeCu-coal gangue heterogeneous activation of peracetic acid for degradation of sulfamethoxazole, J. Environ. Chem. Eng. 11 (2023), 110007.

[62] L. Zhang, J. Chen, Y. Zhang, Y. Xu, T. Zheng, X. Zhou, Highly efficient activation of peracetic acid by nano-CuO for carbamazepine degradation in wastewater: the significant role of H2O2 and evidence of acetylperoxy radical contribution, Water Res 216 (2022), 118322.

[63] J. Lin, Y. Hu, J. Xiao, Y. Huang, M. Wang, H. Yang, J. Zou, B. Yuan, J. Ma, Enhanced diclofenac elimination in Fe(II)/peracetic acid process by promoting Fe (III)/Fe(II) cycle with ABTS as electron shuttle, Chem. Eng. J. 420 (2021), 129692.

[64] J. Lin, J. Zou, H. Cai, Y. Huang, J. Li, J. Xiao, B. Yuan, J. Ma, Hydroxylamine enhanced Fe(II)-activated peracetic acid process for diclofenac degradation: efficiency, mechanism and effects of various parameters, Water Res 207 (2021), 117796.